PERGAMON

International Journal of Solids and Structures 39 (2002) 3857–3872

INTERNATIONAL JOURNAL OF SOLIDS and STRUCTURES

www.elsevier.com/locate/ijsolstr

Experimental characterization of deformation damage in solid polymers under tension, and its interrelation with necking

C. G'Sell *, J.M. Hiver, A. Dahoun

Laboratoire de Physique des Matériaux (UMR CNRS 7556), Ecole des Mines de Nancy (INPL), Parc de Saurupt, 54042 Nancy, France

Received 13 February 2002

Abstract

In many polymers, including glassy thermoplastics and reinforced blends, it has been shown qualitatively that damage processes (crazing and cavitation) contribute to the apparent plastic deformation in addition to shear yielding. The aim of this paper is to determine more quantitatively their influence on the constitutive equation and/or on the kinetics of plastic instability. By using a novel video-controlled testing system, the evolution of volume strain is determined in polyethylene terephtalate (PET) and high-impact polystyrene (HIPS) by measuring in real time the three principal strain components in a small volume element, while the specimens are deformed under uniaxial tension at constant true strain rate. The contribution of volume strain to the overall true strain is 50% in the case of PET and nearly 100% for HIPS. Observation of sample geometry during complementary stretching tests at constant elongation rate show that necking is moderate in PET and completely absent in HIPS, although both polymers undergo stress drop at yield and nearly no strain hardening. This unexpected plastic stability is shown to be due to damage. In this scope, the classical theory of diffuse necking in polymers is revisited in order to take explicitly into account the damage rate, D, which expresses the slope of the volume strain vs. true strain curve.

Keywords: Polymer stretching; Damage; Volume strain; Plastic instability; Necking criterion

1. Introduction

Although the mechanical properties of solid polymers have been the object of much interest from the very beginning of their industrial development, it is only since the 60s that Vincent (1960) introduced the concept of intrinsic plastic behavior. Subsequently, Meinel and Peterlin (1971) and later G'Sell et al. (1983) established a quantitative correlation between the constitutive equation and the dramatic necking process that most ductile polymers undergo upon stretching. Under uniaxial tension, Marquez-Lucero et al. (1989) showed that plastic instability is nucleated immediately after the yield point due to weak consolidation (or even softening), while neck stabilization and propagation is favored by the increasing hardening at large

* Corresponding author. Tel.: +33-3-83-58-41-54; fax: +33-3-83-57-97-94.
E-mail address: gsell@mines.u-nancy.fr (C. G'Sell).

0020-7683/02/$ - see front matter
PII: S0020-7683(02)00184-1

strain. Furthermore, the relatively large strain-rate sensitivity (viscosity) of polymers dampens the growth kinetics of plastic instabilities.

These particular features of polymer behavior have been ascribed to specific microstructural mechanisms. In the case of amorphous polymers, Argon (1973) and Bowden and Raha (1974) have shown that the yield point is associated with the thermally activated overcoming of van der Waals interaction enthalpy between neighboring macromolecules. In several polymers, e.g. polyethylene terephtalate (PET), the material is capable of undergoing extensive plasticity at room temperature. Deformation is seen to localize in fine shear bands which grow and multiply within the neck. As for the strain hardening of glassy polymers, it was interpreted by Arruda and Boyce (1990) in terms of the entropic forces necessary to orient the macromolecular chains connected by cross-links or entanglements. In addition to these cohesive deformation mechanisms, several damage processes play a significant role in the net deformation kinetics of polymers. Crazing of glassy thermoplastics, which represents an important class of such mechanisms, was carefully studied by Kramer (1983) and by many other authors.

Since some glassy polymers, like polystyrene (PS), are too brittle to undergo significant plasticity at room temperature, chemical engineers have designed polymeric "alloys" by blending them with elastomers in view of upgrading their toughness. High-impact polystyrene (HIPS) is one of these materials, described with some details by Sperling (1997). Its specific morphology is made of complex polybutadiene (PB) nodules in the PS matrix. Thanks to its large strain at rupture, HIPS is eligible to structural applications. It has been shown qualitatively that damage mechanisms are very active in HIPS under tension, namely cavitation in the rubbery phase, crazing at the nodule interface and microcracking within the matrix.

Although experimental evidence have proved the important role of non-cohesive mechanisms in the deformation of glassy polymers and blends, most authors after Sternstein (1975) have limited their investigation to crazing vs. shear banding criteria. To date, very few data have been published concerning the quantitative contribution of damage mechanisms to large strain plasticity in polymers, unlike in metals for which some significant progress has been made after the work of Gurson (1977). This is partly because available techniques for determining the kinetics of decohesion within the material during the course of tensile tests were inefficient. Mechanical extensometers were developed to measure simultaneously the strains in the three directions of space, but: (i) they are complicated to manipulate, (ii) they are likely to notch the polymer, (iii) they cannot undergo high temperatures and furthermore, (iv) they are not applicable to materials which exhibit necking, since their calibrated reference volume is much larger than the zone affected by plastic instability. Due to this situation, mechanical behavior of polymers was traditionally analyzed under the simplistic assumption of isochoric deformation, i.e. within a scheme of constant volume plasticity.

Thanks to a novel technique capable of assessing volume changes in real time during the deformation of polymers, we have analyzed the influence of damage mechanisms in a glassy polymer and a polymeric alloy. The aim is to measure the dilatation of a small volume of polymer within a neck. Details of an operational system will be presented, and the plastic response of two polymers (PET and HIPS) will be analyzed in terms of cohesive and non-cohesive strains. On the basis of this information, the theory of necking will be revisited in order to introduce the contribution of damage processes.

2. Experimental procedures

2.1. Materials

Two materials were investigated for this work. The first one is a commercial grade of PET, manufactured by Eastman Chemicals under the reference Eastapak 9921. It is characterized by a number-average molar

mass $M_n = 26,000$ g/mol. The specimens are molded by injection in the shape of 6 mm thick samples. Thanks to the high cooling rate of the PET in the injection process, the polymer is almost completely amorphous, as checked by the conventional technique of differential scanning calorimetry reviewed by Ghijsels and Waals (1980). Its glass transition temperature, T_g, is equal to 75 °C.

The second material is a commercial grade of HIPS, manufactured by Atochem under the reference PS 4241, and molded by injection into 4.1 mm thick samples. In this material, the dispersed rubberlike phase, PB, is polymerized in situ with the PS in a proportion of 7% in weight. The resulting morphology (usually called "salami" morphology) was described by Sperling (1997). The matrix is pure PS with a weight-average molar mass of about 200,000 g/mol. The reinforcing nodules, about 2 μm in diameter, are mainly constituted with PB but contain themselves some droplets of PS. Both PS and PB are amorphous. At room temperature, the PS matrix is glassy ($T_g = 100$ °C), and the PB is rubbery ($T_g = -106$ °C).

In both cases, the processing has been performed with minimum shear rate in the melt and moderate thermal shock on cooling. Consequently, the initial state is fairly isotropic and no significant internal stresses are frozen. This is confirmed to some extent by the negligible birefringence effects observed in the transparent PET samples between crossed polarizers and, for both polymers, by the fact that machining the samples causes no significant distortions which could have been awaited if chain orientation and/or internal stresses were present.

2.2. Video-controlled tensile tests

For this work, we have developed a special video-controlled tensile testing method, in such a way that the constitutive stress–strain behavior and the volume changes could be determined at the same time. It constitutes a new version of the VideoTraction© system (Apollor, Vandoeuvre, France). By contrast to the previous version of the system, described elsewhere by G'Sell et al. (2000), which was limited to materials deforming homogeneously, the present device is now applicable to materials which exhibit "diffuse" necking during a tensile test. This type of plastic instability corresponds to the symmetrical reduction of cross-section caused by the concentration of tensile deformation in a given portion of the specimen. It excludes the case of coarse deformation bands which sometimes develop obliquely to the tensile axis.

For the video-controlled tests, the samples are prepared in the following way. Parallelepipeds are carefully machined out of the plates with overall dimensions of $63 \times 12 \times 6$ mm^3 for PET, and $63 \times 12 \times 4$ mm^3 for HIPS. In order to localize the deformation in the region where all the mechanical variables are determined, a geometric defect is machined in the center of the specimens. The defect, which extends over a length of 13.1 mm (for PET) and 10 mm (for HIPS), correspond to a reduction of width and thickness for PET, and width only for HIPS, with a rounded profile. Consequently, the minimum cross-section is a rectangle of 10.6×4.6 mm^2 for PET and 9.7×4.1 mm^2 for HIPS.

Seven ink markers are printed on the front surface prior to deformation (Fig. 1) and analyzed during the tensile test in order to characterize the plastic behavior locally. The markers are black, nearly round, with a diameter about 0.4 mm. The five markers (A, B, C, D, E) aligned along the tensile axis $\mathbf{x}_3$, the distance between the centers of successive markers being equal to about 1 mm. The three markers (F, C, G) aligned along the transversal axis $\mathbf{x}_1$ are more widely separated, in such a way that they occupy a major fraction of the total width in the geometric defect. The diagram in Fig. 2 is a real photograph of a set of seven markers on a PET sample after some amount of deformation. The aim of the method is to determine the three principal components of strain, ε_1, ε_2 and ε_3, in a proper representative volume element (RVE) of the material where stresses and strains should be nearly uniform. The latter condition is approached near the median cross-section of the neck where markers F, C and G are printed. Since the alignment of these dots perpendicularly to the tensile axis is not perfect, one may qualitatively consider that the light gray slice in

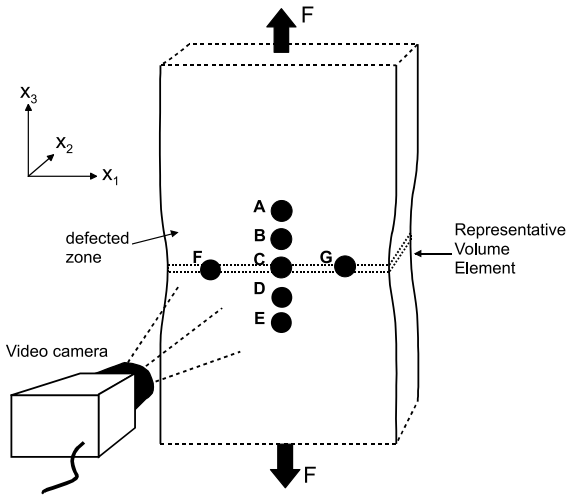

Fig. 1. Configuration of the seven markers in the video-controlled tensile testing system.

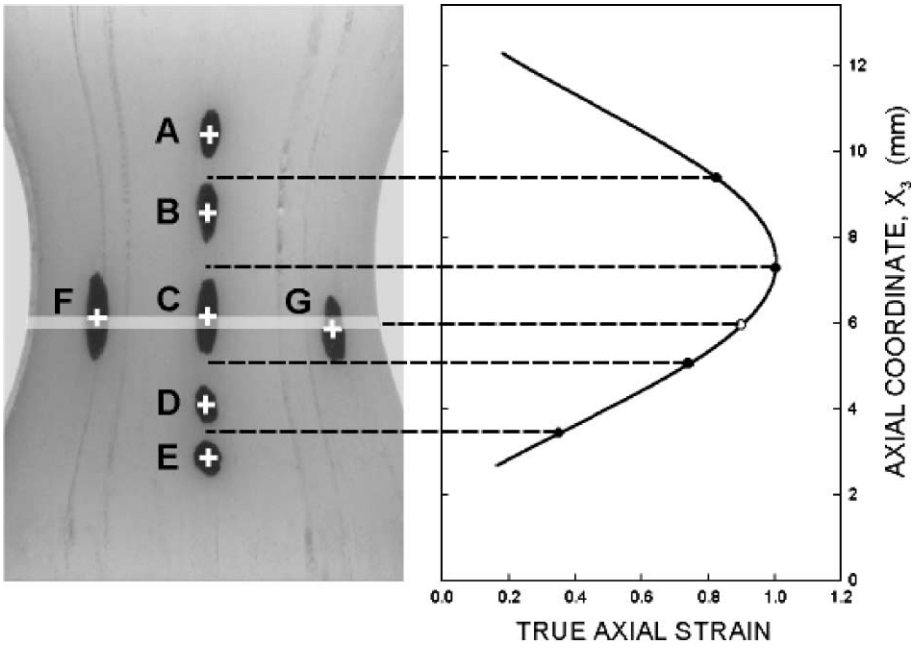

Fig. 2. Configuration of the seven marker set in the case of a PET sample stretched at room temperature, and determination of true axial strain in the elementary representative volume (in light gray).

Fig. 2, whose thickness is 0.2 mm, represents a reasonable RVE in which the material behavior can be defined correctly.

Let us consider first the axial strain distribution. For each one of the marker pairs AB, BC, CD, and DE, we define the axial "true" strain (Hencky strain) by relations of the following type:

$$\begin{aligned}\varepsilon_3(\mathrm{AB}) &= \ln(\mathrm{AB}_3/\mathrm{AB}_{30})\\ \varepsilon_3(\mathrm{BC}) &= \ln(\mathrm{BC}_3/\mathrm{BC}_{30})\\ \varepsilon_3(\mathrm{CD}) &= \ln(\mathrm{CD}_3/\mathrm{CD}_{30})\\ \varepsilon_3(\mathrm{DE}) &= \ln(\mathrm{DE}_3/\mathrm{DE}_{30})\end{aligned} \tag{1}$$

where (AB_{30}, BC_{30}, CD_{30}, DE_{30}) and (AB_3, BC_3, CD_3, DE_3) are the initial and current distances (along $\mathbf{x}_3$) of the centers of gravity of the two markers in the pairs. This axial true strain is attached to the x_3 coordinates of the midpoints of the pairs. As illustrated in Fig. 2 in the practical case of a PET sample, the axial true strain, ε_3, at the level of the RVE can be obtained by non-linear interpolation from the four values of the axial strain along the axis. The precision in the assessment of ε_3 is equal to about 2×10^{-4}.

The second step concerns the transversal true strain ε_1 in the RVE, which is obtained from the marker pair FG with the same Hencky approach by the relation:

$$\varepsilon_1 = \ln(\mathrm{FG}_1/\mathrm{FG}_{10}) \tag{2}$$

where FG_{10} and FG_1 are the initial and current distances (along $\mathbf{x}_1$) of the centers of gravity of the two markers in the FG pair. Actually, in the system developed for this work, it was chosen to determine ε_1 as the average of the strains calculated from the two pairs FC and CG. This procedure is equivalent to the one in Eq. (2) but it presents the interest to allow the operator to verify in real time that the transverse strain is homogeneous across the sample, by checking that the condition $\mathrm{FC}_1/\mathrm{FC}_{10} = \mathrm{CG}_1/\mathrm{CG}_{10}$, is actually fulfilled. Significant artifacts were encountered with polymers (not PET nor HIPS) in which plastic deformation develop in very coarse shear bands oriented obliquely on the tensile axis. The system is thus equipped with a "warning flag" which alerts the user to problematic inhomogeneities of the transversal strain.

As for the second transversal strain, ε_2, it is simply taken equal to ε_1, by assuming that the strain tensor is transversally isotropic. This involves not only that the original microstructure of the material is isotropic, but also that no artifact should favor deformation along one of the two directions $\mathbf{x}_1$ and $\mathbf{x}_2$. Such a situation could arise for example if the specimen is too wide along $\mathbf{x}_1$ with respect to the thickness along $\mathbf{x}_2$. The loading path would then approach the case of "plane strain tension" for which it is well known that the sample deforms more readily through the thickness. The transversal isotropy constraint could be alleviated in the previous system of G'Sell et al. (2000) by analyzing simultaneously markers printed on both lateral faces of the tensile sample but this solution is not readily applicable when necking occurs.

Subsequently, since the three components of strain are defined in the same RVE, the trace of the tensor can be calculated. It is called "volume strain" since it measures the dilatation (or contraction) of the RVE:

$$\varepsilon_\mathrm{v} = \varepsilon_1 + \varepsilon_2 + \varepsilon_3 = \ln(V/V_0) \tag{3}$$

The final precision on the determination of volume strain is equal to about 10^{-3}.

The appropriate stress definition associated with the Hencky strain is the Cauchy stress (often called "true" stress). It takes into account the reduction of the cross-sectional area, $A < A_0$, undergone by the specimen while it is stretched:

$$\sigma_3 = F/A = (F/A_0)\exp(-\varepsilon_1 - \varepsilon_2) \tag{4}$$

The diagram in Fig. 3 illustrates the main features of the VideoTraction© system, and particularly its three interfaces with: (i) the video camera, (ii) the load cell and (iii) the servohydraulic actuator of the tensile testing machine (MTS 810). The first interface acquires the centers of gravity of the seven markers with a frequency of about 30 frames/s, from which it determines the true axial strain ε_3 and the volume strain ε_v. The second interface gives access at the same frequency to the true stress σ_3. The latter interface adjusts continuously the speed of the actuator in such a way that the axial true strain rate, $\dot{\varepsilon}_3 = \mathrm{d}\varepsilon_3/\mathrm{d}t$, is kept constant during the test.

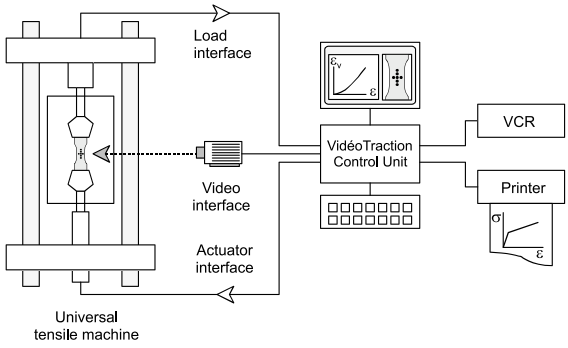

Fig. 3. General diagram of the VideoTraction© system.

Note that the total procedure remains valid even if the viewing direction is not strictly orthogonal to the specimen surface (that is in case of camera disorientation) since the distance ratios involved in the calculation of strains are equal to the ratios of the projected distances. Furthermore, no absolute distance calibration is needed, except for the initial measurement of the specimen cross-sectional area A_0.

Although the method utilized here is applicable in principle for axial strain up to 2.0 or more (that is for local extension ratio larger than 7), it sometimes suffers from artifacts at very large strains in unfavorable cases when: (i) the markers are fragmented, (ii) the distribution of strain across the RVE cross-section becomes non-uniform. The influence of these parameters will receive more attention in forthcoming papers on highly stretchable polymers like polyethylene, with systematic testing campaigns and comparison with finite-element simulations. However in the present cases, since axial true strain in PET and HIPS does not exceed $\varepsilon_3 = 0.8$ and $\varepsilon_3 = 0.3$ respectively, the method is very robust and seizes correctly the essential features of polymer damage.

2.3. Conventional stretching experiments

In addition to the video-controlled tensile tests, conventional stretching experiments were run at constant elongation rate in order to characterize more specifically the development of necking in PET and HIPS. The calibrated portion of the specimens is parallelepipedic ($50.0 \times 7.7 \times 5.1$ mm^3 for PET and $40.0 \times 8.0 \times 4.1$ mm^3 for HIPS) with a geometric defect in the middle (cross-section lower by 3.5%) over a length of 10.0 mm. The samples were stretched with a MTS 4/ML tensile testing machine with a constant cross-head speed of 2 mm/min. Photographs were taken at incremental times during the tests while the variations of applied load vs. applied elongation were recorded. For these experiments, the results are displayed in terms of nominal stress $\sigma_N = F/A_0$ vs. nominal strain $\varepsilon_N = (L - L_0)/L_0$, where A_0 and L_0 are the nominal cross-section and length of the specimen, respectively.

3. Experimental results

3.1. Characterization of the plastic behavior

The video-controlled tensile tests were performed, for both materials, at ambient temperature (23 ± 1°C) and with a constant true strain rate of 5×10^{-4} s^{-1}. All tests were run up to rupture of the samples.

The results obtained with PET are illustrated in Fig. 4a which shows the evolution of true axial stress vs. true axial strain during a typical tensile test. As frequently described before in the literature, the mechanical

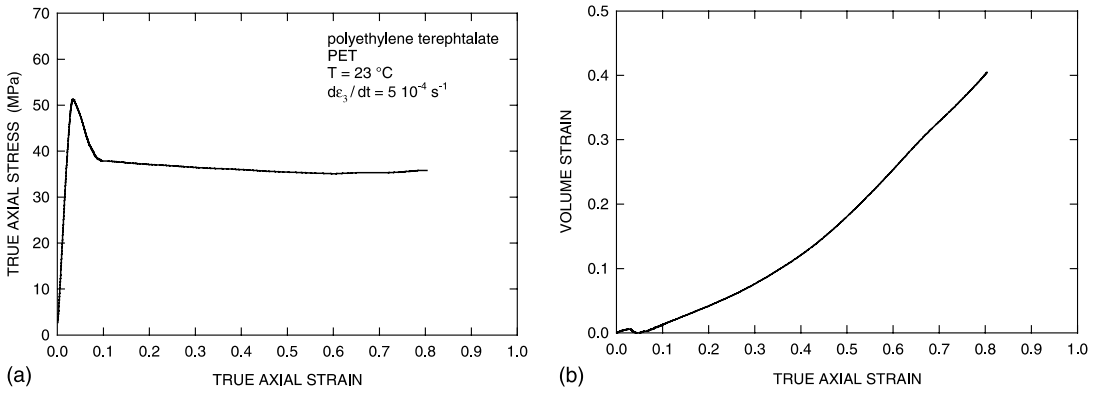

Fig. 4. Mechanical behavior of PET under tensile testing at ambient temperature: (a) stress–strain curve at a constant strain rate of 5×10^{-4} s^{-1}, (b) evolution of volume strain vs. axial true strain.

response of this glassy polymer under monotonous stretching is characterized by a marked yield drop at the elastic limit, while a neck develops at the geometric defect. It should be noted that the stress decrease after yield, about 13 MPa in amplitude, corresponds here to the intrinsic softening of the polymeric glass and has nothing to do with any geometric artifact since the decrease of cross-section at the neck is already taken into account in the definition of true stress. The shear yielding process which mainly controls plastic yielding of PET has been well documented in the literature, after the pioneering work of Bowden and Jukes (1972): bundles of very thin shear bands are nucleated from the external surface, propagate toward the interior, and eventually coalesce in order to reach a nearly uniform deformation after some amount of axial strain. It is noted that the abrupt yield drop terminates after an accumulated strain of about 0.09, and then a long stage of plastic flow begins. Conversely to other glassy polymers for which a definite hardening is recorded, the PET investigated here flows at a nearly constant true stress, even with a small decrease of the true stress. This process continues until the specimen reaches an axial true strain of 0.8, that is for an extension ratio of about 2.2. Other tensile tests were performed with PET with different strain rates, ranging from 5×10^{-5} to 5×10^{-3} s^{-1}. They were used to assess the strain-rate sensitivity coefficient of the material: it is found that the strain-rate sensitivity coefficient, $m = [\partial \ln \sigma_3 / \partial \ln \dot{\varepsilon}_3]_{\varepsilon_3}$, is equal to about 0.035, which is a normal value for a glassy polymer at a temperature not too far below the glass transition.

Resulting from the novel capabilities of the video-controlled testing method presented in Section 2.2, the graph of Fig. 4b shows the evolution of volume strain in the same volume element of PET as the one considered for the stress–strain curve in Fig. 4a. It is seen that a small dilatation occurs in the elastic stage. Although its amplitude is less than 0.01, this phenomenon seems significant with respect to the absolute precision of the ε_v determination is of the order of 10^{-3}. It corresponds to the classical dilatation effect of elastic solids, the Poisson's ratio of the material being given by $\nu = (1 - d\varepsilon_v/d\varepsilon_3)/2$. The analysis of test data gives the classical value: $\nu \approx 0.4$. More interesting is the decrease of volume strain during the stress drop after the yield point. This phenomenon has the net effect to canceling completely the elastic dilatation although the applied stress drops by 25% only. It is the object of intensive experimental and modeling work in this laboratory and will be described in details in a future publication. It is due to macromolecular orientation due to the onset of plastic deformation. Whatever the small volume fluctuations observed in the elastic and yield stages, the major effect observed in Fig. 4b is certainly the considerable volume strain development which starts at a strain of about 0.05 and monotonously increases up to rupture, even at an accelerated rate after a true axial strain of 0.4. Eventually, when the material reaches its rupture strain at $\varepsilon_3 \approx 0.8$, volume strain is as large as $\varepsilon_v \approx 0.4$, which means that non-cohesive deformation mechanisms

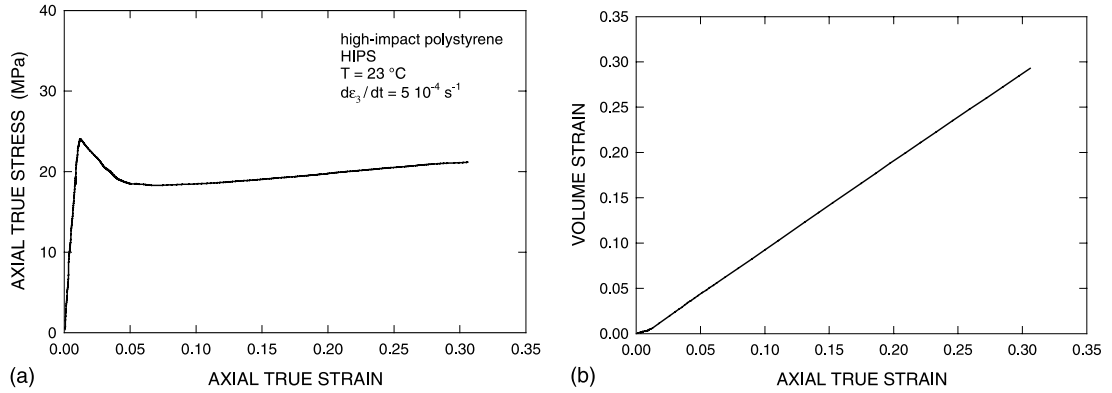

Fig. 5. Mechanical behavior of HIPS under tensile testing at ambient temperature: (a) stress–strain curve at a constant strain rate of 5×10^{-4} s^{-1}, (b) evolution of volume strain vs. axial true strain.

support half the total plastic strain of the material. If one defines the "damage rate" as the slope $D = [\partial\varepsilon_v/\partial\varepsilon_3]_{\dot{\varepsilon}_3}$, one gets $D \approx 0.3$ in the strain interval between 0.05 and 0.4, and then $D \approx 0.73$ in the interval between 0.4 and rupture. In terms of the "tangent Poisson's ratio", $\nu_T = (1 - D)/2$, one gets $\nu_T \approx 0.35$ and $\nu_T \approx 0.14$ in the two intervals identified above. Evidently, this situation is very far from the commonly accepted isochoric assumption which corresponds to $D = 0$, that is to $\nu_T \approx 0.5$.

For the HIPS, the true stress–strain curve displayed in Fig. 5a shows apparent similarity with the case of PET. One notes again the typical features of glassy polymers: initial viscoelastic stage, a marked yield drop and a considerable plastic stage with a slightly positive slope, terminating at fracture for a strain of about 0.3. Although HIPS is less ductile than PET, it is remarkable how the introduction of PB has changed the natural properties of the parent polymer, PS, which normally undergoes brittle fracture at room temperature. By contrast, HIPS shows significant ductility. This is obtained at the price of a certain decrease of the Young's modulus (about 2/3 of the modulus for neat PS). Also, the apparent yield stress of HIPS is relatively modest (24 MPa to be compared with 51 MPa for PET). As for the plastic stage, it is not as developed as for PET, but it provides enough toughness the material to be utilized for many structural applications. Also different tests were run at various strain rates: it is found that the strain-rate sensitivity coefficient is equal to $m = 0.043$ in this material.

Although the stress–strain behavior of HIPS is very similar to one of PET, the graph in Fig. 5b shows that its volume strain is much larger. Except during the viscoelastic stage where a conventional Poisson's effect is observed, an intense dilatation process begins as soon as the yield point is passed. There is even no decrease of the volume strain as the stress drops during the short softening stage after yield point. One can note that the ε_v vs. ε_3 curve is nearly a straight line, the slope damage rate being equal to $D = 0.98$ (and the tangent Poisson's ratio, $\nu_T = 0.01$). It is thus obvious that the plasticity of HIPS is essentially supported by non-conservative mechanisms (crazing, cavitation, decohesion, etc.) and nearly not by plastic shearing.

3.2. Observation of plastic instability

The results of the conventional tensile tests on PET and HIPS will be now examined, in order to characterize the degree of inhomogeneity of deformation and to identify the microstructural processes.

In the experiment with PET, the nominal stress–strain curve (Fig. 6a) shows first a viscoelastic range up to the yield point. During this stage, deformation is nearly homogeneous. Just at yield (photograph at $\varepsilon_N = 0.04$ in Fig. 6b), two shear bands with a dark contrast are hardly observed along the left side of the

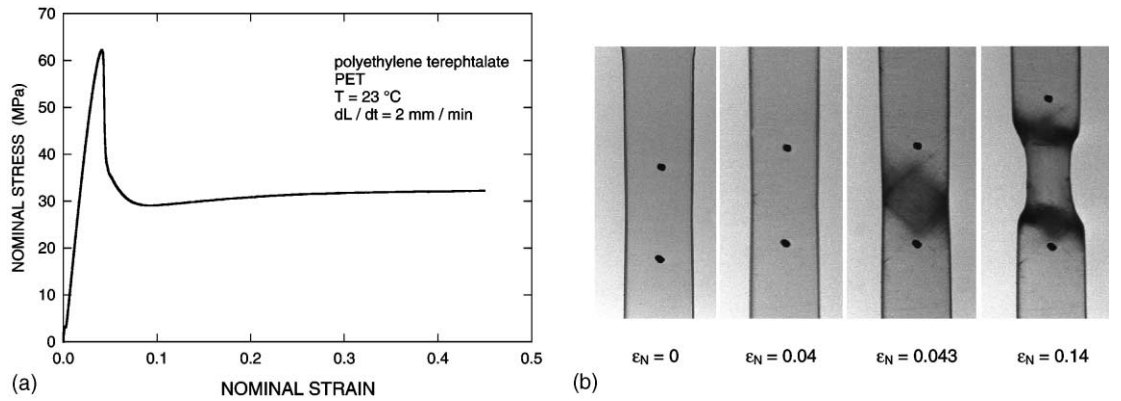

Fig. 6. Stretching behavior of PET under tensile testing at ambient temperature: (a) nominal stress–strain curve at a constant cross-head speed of 2 mm/min, (b) photographs of the sample (the black markers are originally distant of 10 mm).

sample, in the center of the geometric defect. A very abrupt load drop is then observed, with a decrease of nominal stress from 62 to 29.1 MPa. During this critical stage, which lasts only 80 s, plastic yielding propagates across the entire width of the sample. Thanks to the initial transparency of the material, careful examination of the specimen (for example in the photograph at $\varepsilon_N = 0.043$) that the deformation process involves two mechanisms: (i) narrow bands, inclined on the tensile axis, which elongate and multiply gradually and (ii) loss of transparency of the material. The latter phenomenon appears as darkening in this experiment since the sample is observed under rear illumination, but it would appear as whitening if the sample were observed with reflected light. After the nominal stress has stabilized at the plateau (for $\varepsilon_N > 0.09$) a stable "cold drawing" stage takes place, as illustrated by the photograph at $\varepsilon_N = 0.14$. It appears that the center of the neck is less dark that before (probably because the sample got much thinner in this zone), while the shoulders of the neck look like the borders of the dark zone in the preceding micrograph. By the same time, new shear bands nucleate ahead of the necked zone, for example near the lower left side of the specimen, probably induced by some surface scratches formed when machining.

The microstructural processes responsible for localized deformation of PET were characterized, after unloading in samples stretched until the neck propagation stage. Observations were performed by transmission optical microscopy (by means of a polarized Olympus BHS microscope) and also by scanning electron microscopy (with a JEOL SEM 820 microscope). The optical micrograph of Fig. 7, obtained in the border of the neck, shows clearly the activation of both crazes and shear bands. The crazes are perpendicular to the tensile axis. They are about 100 μm long on average and their thickness is too small to be resolved. The shear bands are inclined about 45° on the tensile axis and form a network of lines across the specimen. It is interesting that shear bands seem very often to start and finish near craze tips. This was already observed by G'Sell (1988) on the deformation of PET films. It is not clear whether crazes are nucleated at the intersection of pre-existing shear bands or, on the contrary, if shear bands are preferably nucleated from the tips of crazes due to the local stress concentrations. The second assumption seems more correct since optical micrographs obtained further ahead of the darkened zone show early crazes and no shear bands. Optical microscope being unable to resolve any microstructural feature in the center of the neck, scanning electron microscope (SEM) was used to study this region. The micrograph in Fig. 8 was thus obtained in a zone which had undergone a true axial strain of $\varepsilon_3 \approx 0.5$. The material was abraded with sand paper in order to expose the interior of the sample, and eventually polished with diamond paste to remove scratches. Also the small slab such obtained was gently bent with a jig on the microscope stage in order to open the defects created during the tensile test, if any (it was checked with a reference undeformed specimen that the bending jig did not

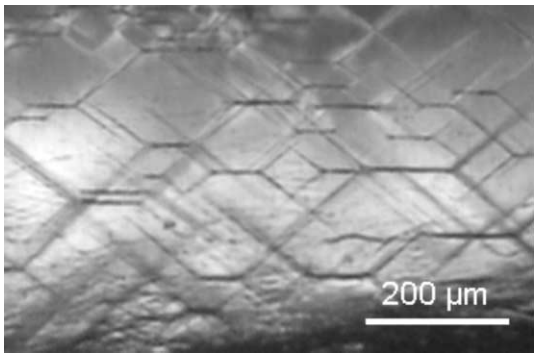

Fig. 7. Transmission optical micrograph of shear bands and crazes in the shoulder of the neck, in a PET sample under uniaxial tension (the tensile axis is vertical).

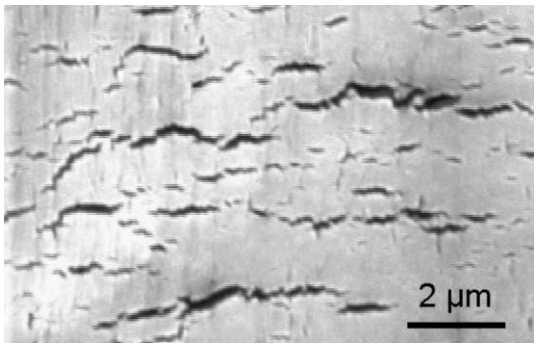

Fig. 8. Scanning electron micrograph of crazes in the center of the neck, in a PET sample under uniaxial tension (the tensile axis is vertical).

produce new crazes). At this scale, the micrograph shows a collection of discontinuous crazes, about 1 μm in length, oriented grossly perpendicular to the tensile axis. The maximum width of the crazes is of the order of 200 nm. As shown previously (G'Sell, 1988), the shear bands which do exist in sample deformed at such large strains are not properly revealed by SEM.

As shown in Fig. 9, the case stretching behavior of HIPS is very different. The nominal stress–strain curve shows much less instability than for PET. Even if a definite yield drop is observed, the amplitude of this drop is very limited, not more than 4.5 MPa. The most remarkable feature for this material is that there is almost no necking in the specimen while stretched (see photographs in Fig. 9b). This is in good agreement with the results of the video-controlled tests in Fig. 5 from which it was concluded that the HIPS deform entirely by craze opening, and not by shear processes. Even when the sample has reached an elongation of 30% at rupture, it exhibits no change of its cross-sectional area as compared with the initial value. Furthermore, visual examination of the specimen surface clearly shows significant whitening of the material under reflected light (this phenomenon is hardly visible in Fig. 9b due to the poor contrast of the photographs), which confirm the important damage activity. However, since HIPS is opaque due to the diffusion of transmitted light by PB nodules, it is not possible to determine by optical microscopy which type of damage process is dominant. Many authors, e.g. Keskkula and Schwarz (1986), have reported electron microscopy observations (TEM or SEM) which show that the extensive volume change of HIPS upon

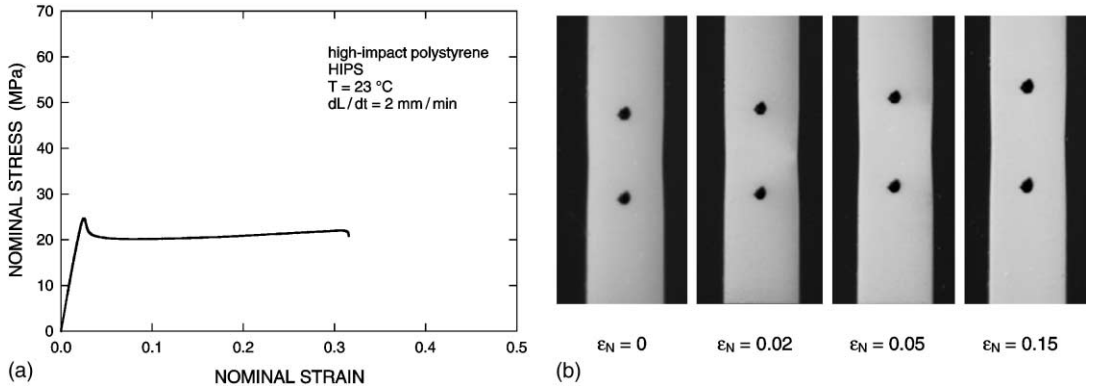

Fig. 9. Stretching behavior of HIPS under tensile testing at ambient temperature: (a) nominal stress–strain curve at a constant cross-head speed of 2 mm/min, (b) photographs of the sample (the black markers are originally distant of 10 mm).

plastic deformation results in the combination of crazing in the PS matrix, decohesion at the PS/PB interface and cavitation in the PB nodules. This profuse multiplication of defects in HIPS is precisely the cause of its considerable toughness since the energy consumed by these damage mechanisms is not available for the dangerous propagation of major cracks.

4. Modeling of plastic instability under tension in craze forming

4.1. Motivation of the investigation

Since Ward (1971) proved that deformation induced orientation was likely to improve the rigidity and elastic limit of macromolecular materials (and, by the way, makes them eligible for high-value structural applications), many authors have tried to predict and optimize the stretching behavior of solid polymers. The process of diffuse necking, in particular, received much attention and was the object of some controversy over the parameters which control its development. Considerable progress was made when several authors, like G'Sell (1988), proved that the kinetics of neck formation and propagation could be modeled and predicted quantitatively from the constitutive equation of the material expressed in terms of true stress, true strain and true strain rate. Nowadays, this concept is broadly acknowledged, and plastic instability phenomena are thus modeled in complex structures for industrial products by means of finite-element codes. This is the reason why there is such a large need for databases giving the intrinsic parameters of polymers up to large strains.

On this way toward the correct modeling of plastic behavior, the importance of the volume change effects has been largely underestimated, or even completely ignored. This is because, following conclusions obtained for metals, most theories consider that plasticity in polymers is essentially controlled by isochoric shear banding mechanisms. Even though most workers know the literature on crazing or cavitation, and are aware of the dilatation caused by these processes, the volume variations during plastic deformation are generally neglected in practical applications. The results presented in the preceding section prove that the isochoric approximation is not justified a priori. Complementary experiments performed by the authors on other polymers (to be published later) proved that PET and HIPS are not exceptions, and that most ductile polymers exhibit significant damage as well.

The aim of the following section will be to revisit the bases of the well-known theory of plastic instability in order to take into account in a reasonably simple way the effect of strain-induced volume changes on plastic instability in polymers.

4.2. Kinetics of plastic instability in a damaging material

For this analysis, we will restrict our purpose to the development of diffuse necks in uniaxial tensile specimens. This limitation will of course exclude from the model the case of obliquely localized shear bands. Therefore, one should consider that the equations derived below as a preliminary approach to the problem, whose aim is mainly to introduce new pertinent parameters in the model. We are conscious that the treatment of more realistic cases will necessitate the use of refined mechanical tools, but those are outside the scope of this work.

Like Semiatin and Jonas (1984), we will restrict our study to the case of steady-state stretching and short samples, so that both effects of inertia and gravity will be neglected. Consequently, the tensile force F is transmitted along the specimen axis:

$$F = \sigma_3(X_3)A(X_3) = \text{const.} \tag{5}$$

In the above expression, $\sigma_3(X_3)$ is the current true axial stress and $A(X_3)$ the current cross-section. The X_3 coordinate, oriented toward the center of the initial defect, measures the *lagrangian* position of a material slice, as in the analysis of G'Sell et al. (1985). With this definition, the distance δX_3 between two material elements does not vary during deformation, as opposed to the *eulerian* distance δx_3 (usual laboratory coordinate) which increases with the local strain ε_3 following the expression $\delta x_3 = \delta X_3 \exp(\varepsilon_3)$. Eq. (5) rewritten with logarithmic derivatives is:

$$\left[\frac{\delta \ln \sigma_3(X_3)}{\delta X_3}\right]_t + \left[\frac{\delta \ln A(X_3)}{\delta X_3}\right]_t = 0 \tag{6}$$

At constant temperature, the variation of true axial stress $\sigma_3(X_3)$ along the specimen results from the variations of strain, ε_3 and strain rate $\dot{\varepsilon}_3$ and on temperature T. If one admits the existence of an equation of state $\sigma_3(\varepsilon_3, \dot{\varepsilon}_3, T)$, the following equation is obtained:

$$\left[\frac{\delta \ln \sigma_3}{\delta X_3}\right]_t = \left[\frac{\partial \ln \sigma_3}{\partial \varepsilon_3}\right]_{\dot{\varepsilon}} \left[\frac{\delta \varepsilon_3}{\delta X_3}\right]_t + \left[\frac{\partial \ln \sigma_3}{\partial \ln \dot{\varepsilon}_3}\right]_{\varepsilon} \left[\frac{\delta \ln \dot{\varepsilon}_3}{\delta X_3}\right]_t \tag{7}$$

where $[\partial \ln \sigma / \partial \varepsilon]_{\dot{\varepsilon}}$ expresses the derivative of stress with respect to strain at constant strain rate. The above equation gives:

$$\left[\frac{\delta \ln \sigma_3}{\delta X_3}\right]_t = \gamma \left[\frac{\delta \varepsilon_3}{\delta X_3}\right]_t + m \left[\frac{\delta \ln \dot{\varepsilon}_3}{\delta X_3}\right] \tag{8}$$

where γ and m are the coefficients of strain hardening and of strain-rate sensitivity, respectively. The second term in Eq. (5) is linked on one hand to the fluctuations of initial cross-section $A_0(X_3)$, and on the other hand to the variations of current strain $\varepsilon_3(X_3)$, so that one can write:

$$\left[\frac{\delta \ln A}{\delta X_3}\right]_t = \frac{\mathrm{d} \ln A_0}{\mathrm{d} X_3} + \left[\frac{\delta(\varepsilon_1 + \varepsilon_2)}{\delta X_3}\right]_t \tag{9}$$

where the term describing the geometric defect, $\mathrm{d} \ln A_0 / \mathrm{d} X_3$, is expressed with a total derivative term since it expresses the initial state of the specimen.

In the case of a material whose deformation is isochoric, this expression becomes:

$$\left[\frac{\delta \ln A}{\delta X_3}\right]_t = \frac{\mathrm{d} \ln A_0}{\mathrm{d} X_3} - \left[\frac{\delta \varepsilon_3}{\delta X_3}\right]_t \tag{10}$$

but if one considers a material undergoing damage on stretching (that is for a material where $\varepsilon_v = \varepsilon_1 + \varepsilon_2 + \varepsilon_3 \neq 0$), Eq. (10) must be revisited. We introduce in this analysis the damage rate, $D = [\delta\varepsilon_v/\delta\varepsilon_3]_{\dot{\varepsilon}_3}$, so that Eq. (10) is modified to:

$$\left[\frac{\delta \ln A}{\delta X_3}\right]_t = \frac{\mathrm{d}\ln A_0}{\mathrm{d}X_3} - (1-D)\left[\frac{\delta\varepsilon_3}{\delta X_3}\right]_t \tag{11}$$

One defines the "strain gradient", λ, as the local derivative of strain vs. the lagrangian coordinate X_3 at a given time, t, following the equation:

$$\lambda = \left[\frac{\delta\varepsilon_3}{\delta X_3}\right]_t \tag{12}$$

It should be remarked that, in Eq. (8), the second term on the right hand side includes the "strain-rate gradient" in the form $[\delta \ln \dot{\varepsilon}_3/\delta X_3]_t$, which in turn can be rewritten as:

$$\left[\frac{\delta \ln \dot{\varepsilon}_3}{\delta X_3}\right]_t = \frac{1}{\dot{\varepsilon}_3}\left[\frac{\delta \dot{\varepsilon}_3}{\delta X_3}\right]_t = \frac{\partial}{\partial \varepsilon_3}\left[\frac{\delta\varepsilon_3}{\delta X_3}\right]_t = \left[\frac{\delta\lambda}{\delta\varepsilon_3}\right]_t \tag{13}$$

Combining the above equations finally leads to:

$$m\left[\frac{\delta\lambda}{\delta\varepsilon_3}\right]_t = (1-D-\gamma)\lambda - \frac{\mathrm{d}\ln A_0}{\mathrm{d}X_3} \tag{14}$$

One can check that this relation constitutes the differential equation which rules out the evolution of the strain gradient, λ, vs. current true strain, ε_3. It is evident from this equation that the kinetics of plastic instability (i.e. the rate of neck growth) depends on three parameters: (i) the "initiation" parameter, $(-\mathrm{d}\ln A_0/\mathrm{d}X_3)$, which controls the initial localization of strain at the geometric defect, (ii) the strain-rate sensitivity coefficient, m, which acts as a "damping" factor slowing down the variations of strain gradient and, over all, (iii) the "destabilization" factor, $(1-D-\gamma)$, which causes the aggravation or conversely the healing of neck development. While the initiation and damping parameters are positive, the destabilization factor changes its sign according to deformation.

In the past, most theories were based on isochoric plasticity assumption, so that the destabilization factor reduced to $(1-\gamma)$. For polymers G'Sell and Jonas (1979) observed that the hardening coefficient, γ, passes after the elastic limit through a transient stage with $\gamma < 1$ before becoming again larger to unity at some plastic strain usually between 0.6 and 1.2. G'Sell (1988) showed that this specific property of polymers controls their "cold drawing" process. Semiatin and Jonas (1984) showed that $\lambda(\varepsilon_3)$ increases exponentially when the destabilization factor, $(1-\gamma)$, is positive. This explains why necking develops so early in polymers since the latter condition is met just after the elastic limit. Later, the neck stabilizes as soon as $(1-\gamma)$ recovers a negative value. One readily notes that the conditions for neck formation and arrest correspond to the classical Considère criterion $\mathrm{d}\sigma_3/\mathrm{d}\varepsilon_3 = \sigma_3$ which is fulfilled for two distinct strains with polymers. This situation contrasts with the case of metals for which the criterion is reached only once: neck forms at a higher strain (typically $\varepsilon_3 \approx 0.3$ for low carbon steel) but never stabilizes since γ continuously decreases. The original behavior of polymers is due to the stiffening of macromolecular chains when they get oriented on stretching. Furthermore, for polymers which exhibit earlier hardening (for example for those with tightly cross-linked chains), the second Considère point is reached sooner and necking is not so much pronounced.

If we analyze now the case of materials exhibiting damage during plastic deformation, the instability criterion is now expressed through the sign of $(1-D-\gamma)$. In most cases, the damage rate, D, is positive so that the increase of volume strain constitutes a stabilizing factor for necking. The fact that damage promotes deformation stability was not so obvious a priori, but is quite logical if one considers that a specimen with extensive damage elongates with minor change of cross-section. This property received only little

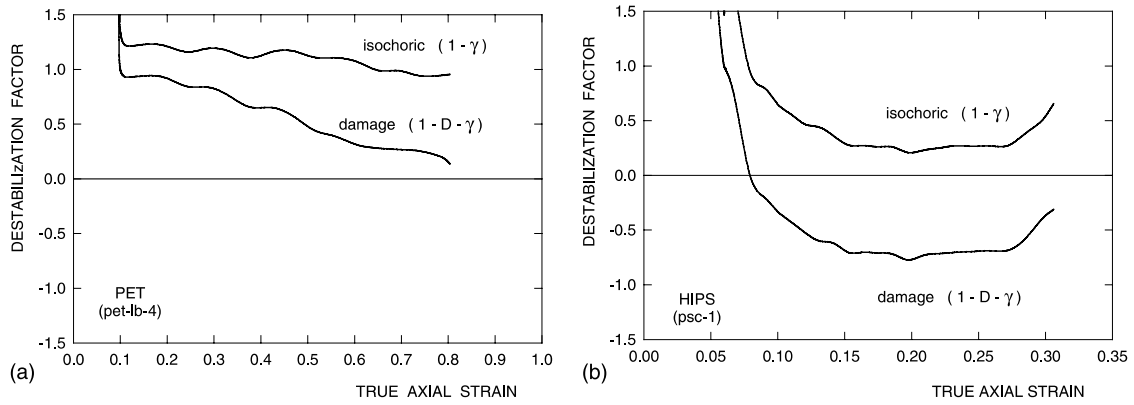

Fig. 10. Evolution of the destabilization factor vs. true strain for isochoric deformation, $(1-\gamma)$, and with damage, $(1-D-\gamma)$: (a) for PET, (b) for HIPS.

attention in the literature on metals since the contribution of volume strain to the overall plastic strain is usually very small for those materials. By contrast, for polymers, the stretching behavior is much more influenced by damage processes.

In order to discuss more quantitatively the above arguments, we have plotted in Fig. 10 the variations of the destabilizing factor for the two polymers under investigation in the case of isochoric deformation, $(1-\gamma)$, and of deformation with damage, $(1-D-\gamma)$. For PET (Fig. 10a), since damage is limited ($D \approx 0.30$ below $\varepsilon_3 = 0.4$ and $D \approx 0.73$ beyond), the destabilization factor remains positive, inducing neck formation as observed in the experiment of Fig. 6b. Only it is noted that the destabilization effect is reduced by an average factor of about 50% with reference to the isochoric case. As for HIPS, the graph of Fig. 10b shows clearly that the important damage undergone by this material ($D \approx 0.98$) has a very efficient stabilizing effect. While the $(1-\gamma)$ curve remains in the positive range, the $(1-D-\gamma)$ curve drops rapidly in the negative range where the neck development is rapidly healed out. The very stable stretching of HIPS observed experimentally (Fig. 9b) is thus predicted with no ambiguity by this theoretical approach. Although several features of this polymeric alloy (sharp yield point, plastic softening, small strain-rate sensitivity) favor plastic instability, it is now evident that the very active crazing mechanisms impede lateral shrinkage of the stretched specimen.

Explicit introduction of damage rate into the constitutive equation of state of the polymers would make possible to predict the behavior of complex structures of these materials by means of finite-element computation. This will be the object of a future work.

5. Conclusions

A novel experimental technique was developed for assessing the contribution of volume strain to the overall plastic behavior of solid polymers upon stretching. Based on the video analysis of a series of seven markers printed on the specimen, this technique is applicable to materials undergoing diffuse necking since the determination of the three principal strains is performed within a very small volume element situated in the center of the neck. Stress–strain behavior could be obtained at constant true strain rate with simultaneous determination of the volume strain.

This technique was applied to PET and HIPS at room temperature. The PET exhibits the typical plastic response of a glassy polymer, with a marked stress drop at yield followed by a steady-state plastic stage up

to a rupture strain of 0.8. Deformation damage by crazing is observed while the material deforms plastically in a neck, causing a significant whitening of the specimen. The volume strain corresponding to this phenomenon increases gradually after a critical tensile strain of 0.05. The volume strain at rupture, equal to 0.4, is thus half the overall true strain. The behavior of HIPS, although similar to the above material to what is concerned by the stress–strain behavior, contrasts significantly in terms of damage and plastic instability. The volume strain for this material is nearly equal to the axial true strain, which means that the specimen is stretched without any lateral contraction. The "plastic" deformation is thus entirely controlled by crazing and cavitation processes, in good agreement with the observations of several authors. Consequently, this polymeric alloy shows no necking despite the yield drop and the low hardening.

The classical theory of plastic instability in polymers, which had been originally established under the simplifying assumption of isochoric plasticity was revisited in order to take into account the important effect of volume strain. This derivation was written in the frame of lagrangian space coordinate in a simple unidimensional approach. It was showed that the development of the strain gradient from an initial geometric defect obeys the same type of differential equation as in the isochoric case. Only the destabilizing coefficient, $(1-\gamma)$, must be change to $(1-D-\gamma)$, where γ is the strain hardening coefficient and D the damage rate. Since it was shown that the growth of plastic instability is triggered by a positive value of the destabilizing coefficient, it arises that the classical Considère criterion, $\gamma < 1$, should be replaced by the new criterion $\gamma + D < 1$ when volume strain plays a significant role. This results unexpectedly means that plastic damage has a definite stabilizing effect on the development of necks in stretched polymers.

Acknowledgements

Part of this paper is based on the laboratory project of J. Etienne at the Ecole des Mines and on valuable scientific discussions with S. Elkoun, on leave from this institution. Both are acknowledged for their respective contribution. The authors are indebted to Eastman Chemical and Atofina Research for kindly providing specimens for the experimental work.

References

Argon, A.S., 1973. A theory for the low-temperature plastic deformation of glassy polymers. Philosophical Magazine 28, 839–865.

Arruda, E.M., Boyce, M.C., 1990. An experimental and analytical investigation of the large strain compressive and tensile response of glassy polymers. Polymer Engineering and Science 30 (20), 1288–1298.

Bowden, P.B., Jukes, J.A., 1972. The plastic flow of isotropic polymers. Journal of Materials Science 7, 52–63.

Bowden, P.B., Raha, S., 1974. A molecular model for yield and flow in amorphous glassy polymers making use of a dislocation analogue. Philosophical Magazine 29, 149–166.

Ghijsels, A., Waals, F.M., 1980. Differential scanning calorimetry: a powerful tool for the characterization of thermoplastics. Polymer Testing 1, 149–160.

G'Sell, C., 1988. Instabilités de déformation pendant l'étirage des polymères solides. Journal de Physique III 23, 1085–1101.

G'Sell, C., Jonas, J.J., 1979. Determination of the plastic behavior of solid polymers at constant true strain rate. Journal of Materials Science 14, 583–591.

G'Sell, C., Aly-Helal, N.A., Jonas, J.J., 1983. Effect of stress triaxiality on neck propagation during the tensile stretching of solid polymers. Journal of Materials Science 18, 1731–1742.

G'Sell, C., Hiver, J.M., Gehin, F., 2000. Real-time quantitative determination of volume variations in polymers under plastic strain. In: Deformation, Yield and Fracture of Polymers. The Institute of Metals, London, pp. 371–374.

G'Sell, C., Marquez-Lucero, A., Gilormini, P., Jonas, J.J., 1985. Flow localization and determination of constitutive relations in highly drawn polymers: one dimensional eulerian formulation of the effect of stress triaxiality. Acta Metallurgica 33, 759–770.

Gurson, A.L., 1977. Continuum theory of ductile rupture by void nucleation and growth, Part I—Yield criteria and flow rules for porous ductile media. Journal of Engineering Materials and Technology 99, 2–15.

Keskkula, H., Schwarz, P.D.R., 1986. Examination of failure in rubber toughened polystyrene. Polymer 27, 211–216.

Kramer, E.J., 1983. Microscopic and molecular fundamentals of crazing. In: Kausch, H.H. (Ed.), Crazing in Polymers. Advances in Polymers Science, vol. 52/53. Springer-Verlag, Berlin, pp. 1–56.

Marquez-Lucero, A., G'Sell, C., Neale, K.W., 1989. Experimental investigation of neck propagation in polymers. Polymer 30, 636–642.

Meinel, G., Peterlin, A., 1971. Plastic deformation of polyethylene II. Change of mechanical properties during drawing. Journal of Polymer Science: Part A2 9, 67–83.

Semiatin, S.L., Jonas, J.J., 1984. Instability and flow localization in uniaxial tension. In: Formability and Workability of Metals. ASM, Metals Park, OH, pp. 149–198.

Sperling, L.H., 1997. Rubber toughening of engineering plastics. In: Polymeric Multicomponent Materials. Wiley, New York, NY, pp. 223–274.

Sternstein, S.S., 1975. Yielding modes in glassy polymers. In: Polymeric Materials. ASM, Metals Park, OH, pp. 369–410.

Vincent, P.I., 1960. The necking and cold-drawing of rigid plastics. Polymer 1, 7–19.

Ward, I.M., 1971. Mechanical Properties of Solid Polymers. Wiley, London.